Applied Catalysis B: Environmental 144 (2014) 29–35

Contents lists available at ScienceDirect

Applied Catalysis B: Environmental

journal homepage: www.elsevier.com/locate/apcatb

Preparation of Cu-doped ZnS QDs/TiO_2 nanocomposites with high photocatalytic activity

Houcine Labiadh[a], Tahar Ben Chaabane[a], Lavinia Balan[b], Nidhal Becheik[c], Serge Corbel[c], Ghouti Medjahdi[d], Raphaël Schneider[c,*]

[a] Unité de Recherche UR11ES30 de Synthèse et Structures de Nanomatériaux, Université de Carthage, Faculté des Sciences de Bizerte, 7021 Jarzouna, Tunisia
[b] Institut de Science des Matériaux de Mulhouse (IS2M), LRC 7228, 15 rue Jean Starcky, 68093 Mulhouse, France
[c] Université de Lorraine, Laboratoire Réactions et Génie des Procédés (LRGP), UMR 7274, CNRS, 1 rue Grandville, BP 20451, 54001 Nancy Cedex, France
[d] Université de Lorraine, Institut Jean Lamour (IJL), UMR 7198, CNRS, BP 70239, 54506 Vandoeuvre-lès-Nancy Cedex, France

ARTICLE INFO

Article history:
Received 14 March 2013
Received in revised form 27 June 2013
Accepted 2 July 2013
Available online 11 July 2013

Keywords:
Cu-doped zinc sulfide
Titanium dioxide
Oxidation
Photocatalysis

ABSTRACT

Cu-doped ZnS quantum dots (QDs) were synthesized in aqueous solution using 3-mercaptopropionic acid (MPA) as stabilizer. Transmission electron microscopy (TEM) results indicate that the Cu:ZnS nanocrystals distribute uniformly and the size is ca. 2.9 ± 0.5 nm. These nanocrystals were successfully associated to anatase TiO_2 nanoparticles to yield TiO_2/Cu:ZnS photocatalysts. Morphological and optical properties of TiO_2/Cu:ZnS nanocomposites were characterized by X-ray diffraction (XRD) analysis, TEM, and UV–vis and fluorescence spectroscopies. Photocatalytic activities of TiO_2/Cu:ZnS nanocomposites were evaluated by the oxidation of salicylic acid aqueous solutions under UV light irradiation. Enhanced performances compared either to pure TiO_2 nanoparticles or to undoped TiO_2/ZnS nanocomposites were observed. Effects of the mass ratio of the TiO_2 and Cu:ZnS and of the pH of the aqueous solution containing salicylic acid on the photocatalytic activities of TiO_2 nanoparticles sensitized with Cu:ZnS QDs were also investigated.

1. Introduction

Over the last years, photocatalytic degradation has received much attention as an alternative method in the removal of environmental pollutants in aqueous phase as well as in gaseous media. Titanium dioxide (TiO_2) was recently confirmed as one of the most potential semiconductor for degradation of unwanted and toxic organic compounds, removal of pollutants in contaminated water and air, and killing of harmful bacteria [1–5]. During photocatalysis experiments with TiO_2, electrons (e^-) and holes (h^+) are generated at the surface of TiO_2 and are converted into excitons in quantum states near the surface after energy relaxation. During this process, a fast e^-–h^+ recombination takes place to form the luminescent exciton states, and thus the charge carriers are not so efficiently transferred to substrate for redox reaction. Among the four polymorphs of TiO_2 found in nature, the anatase phase is the most photoactive because photogenerated charge carriers recombine at the lowest rate in anatase and many organic molecules readily interact with the anatase surfaces [6–8]. To increase the photocatalytic reaction rates, the photogenerated e^- and h^+ must be separated into different locations on the catalyst. This can be achieved by deposition of another semiconductor, generally quantum dots (QDs), at the surface of TiO_2 to form a heterojunction structure and thus enhance the catalytic performance of photocatalysts [9,10]. Once both semiconductors excited by light, e^- accumulate at the low-lying conduction band of one semiconductor while h^+ accumulate at the valence band of the other material. These processes of charge separation are very fast and the efficiency of reduction or oxidation of the adsorbed organics remarkably increases.

TiO_2/CdS [11–14], TiO_2/CdSe [15–17], TiO_2/PbS [18–20] or TiO_2/PbSe [21,22] heterojunctions have been widely studied in recent years to decompose contaminants effectively. This interest is due to the fact that QDs are photostable and that their optic and electronic properties can be adjusted by changing their size and shape. Moreover, CdS, CdSe, PbS or PbSe QDs possess energetically high-lying conduction bands, and can thus prevent e^-–h^+ recombination due to efficient spatial separation of photogenerated charge. However, in view of recent environmental regulations, the high toxicity of cadmium or lead introduces a doubt on the future applicability of this kind of QDs. Thus, several heavy metal-free alternative materials like $CuInS_2$ [23] or $AgGa_{1-x}In_xS_2$ [24] have been proposed to replace Cd- or Pb-based QDs.

Although being a wide band gap semiconductor, ZnS nanocrystals can also be associated to TiO_2 to increase its photocatalytic activity because of their high potentials of conduction band e^- and

* Corresponding author. Tel.: +33 3 83 17 50 53.
E-mail address: raphael.schneider@univ-lorraine.fr (R. Schneider).

0926-3373/$ – see front matter © 2013 Elsevier B.V. All rights reserved.
http://dx.doi.org/10.1016/j.apcatb.2013.07.004

valence band h^+ (−1.75 and +1.85 V versus normal hydrogen electrode) [25,26]. The photocatalytic efficiency of ZnS [27] or TiO_2/ZnS [28–30] has already been demonstrated in various photoreductions or photooxidations. It is also worth to mention that doping of ZnS with Ni^{2+}, Cu^{2+}, Mn^{2+} or Co^{2+} ions favorably shifts the optical response into visible region [31–34].

On the basis of these considerations, in this work we report a study concerning the use of Cu-doped ZnS QDs associated to TiO_2 as photocatalyst. We demonstrate that the TiO_2/Cu:ZnS nanocomposite is an excellent photocatalyst under UV irradiation with markedly improved photodegradation efficiency of salicylic acid compared to TiO_2 or to TiO_2/ZnS nanoparticles.

2. Experimental

2.1. Characterization

Transmission electron microscopy (TEM) images were taken by placing a drop of the particles in water onto a carbon film-supported copper grid. Samples were studied using a Philips CM20 instrument operating at 200 kV equipped with Energy Dispersive X-ray Spectrometer (EDS). The X-ray powder diffraction data were collected from an X'Pert MPD diffractometer (Panalytical AXS) with a goniometer radius 240 mm, fixed divergence slit module (1/2° divergence slit, 0.04 rd Sollers slits) and an X'Celerator as a detector. The powder samples were placed on zerobackground quartz sample holders and the XRD patterns were recorded at room temperature using Cu Kα radiation (λ = 0.15418 nm). X-ray photoelectron (XPS) measurements were performed at a residual pressure of 10^{-9} mbar, using a KRATOS Axis Ultra electron energy analyser operating with an Al Kα monochromatic source.

All the optical measurements were performed at room temperature (20 ± 1 °C) under ambient conditions. Absorption spectra were recorded on a Perkin-Elmer (Lambda 2, France) UV-visible spectrophotometer. Fluorescence spectra were recorded on a Fluorolog-3 spectrofluorimeter F222 (Jobin Yvon, France) equipped with a thermostated cell compartment (25 °C), using a 450 W Xenon light source. Diffuse reflectance ultraviolet and visible spectra of the samples were measured from the optical absorption spectra using a Shimadzu UV-vis-NIR 3600 spectrophotometer. Fine $BaSO_4$ powder is used as a standard for baseline measurements and spectra are recorded in a range of 250–800 nm. ESR experiments were carried out using a X-Band EMX-plus spectrometer (Bruker Biospin). The samples were investigated at room temperature. 2,2,6,6-Tetramethylpiperidine-1-oxyl (TEMPO) was used as calibration standard (g = 2.0061).

A Shimadzu HPLC system equipped with a reversed-phase column (Lichrosorb RP-18) and a UV–vis detector (SPD-20A) was used to detect salicylic acid at 295 nm. The mobile phase was methanol/water acidified with phosphoric acid (70/30, v/v) and the flow rate was 1 mL/min. The column temperature was 25 °C. Twenty microliters of the test solution were injected.

2.2. Materials

Zinc sulfate heptahydrate ($ZnSO_4{\cdot}7H_2O$, 99.99%), copper chloride ($CuCl_2$, 99%), sodium sulfide ($Na_2S{\cdot}9H_2O$, 98+%), 3-mercaptopropionic acid (MPA, 99%), salicylic acid (SA, >99%) and *i*-PrOH (HPLC grade) were purchased from Sigma–Aldrich and used as received without additional purification. TiO_2 P-25 was purchased from Degusa. All solutions were prepared using Milli-Q water (18.2 MΩ cm, Millipore) as the solvent.

2.3. Synthesis of MPA-capped Cu:ZnS and ZnS QDs

For 3% Cu^{2+} doping, Cu:ZnS@MPA QDs are prepared as follows. In a three-neck round-bottomed flask, 5 mL of 0.1 M $ZnSO_4{\cdot}7H_2O$, 150 μL of 0.1 M $CuCl_2$, and 20 mL of 0.1 M MPA were combined. The pH of this solution was adjusted to 11 using 2 M CsOH. Next the solution was degassed by bubbling N_2 gas for 1 h, after which 4.5 mL of degassed 0.1 M $Na_2S{\cdot}9H_2O$ were quickly injected into the solution. The reaction mixture was then brought to reflux. After ca. 12 h heating, the solution was cooled down to room temperature. The colorless solution was then concentrated to the half using a rotating evaporator (50 °C, 15 mmHg), the nanocrystals were precipitated using *i*-PrOH, collected by centrifugation, washed 3 times with *i*-PrOH, and then dried in vacuum at room temperature.

ZnS@MPA QDs were prepared using a similar procedure except that $CuCl_2$ was not added in the reaction medium.

2.4. Preparation of TiO_2/Cu:ZnS nanocatalysts

TiO_2 (800 mg) and Cu:ZnS@MPA QDs (8 mg) were dispersed in 200 mL water and the mixture was sonicated for 15 min and further stirred for 1 h at room temperature. The TiO_2/Cu:ZnS nanocatalyst was recovered by centrifugation and dried overnight at 100 °C in an oven. This annealing did not change the phase of the anatase nanocrystals and of Cu:ZnS QDs.

2.5. Photocatalytic activity

The photoreactor is a self-constructed microreactor [35] with fluorescent lamp (365 nm, I = 1.5 mW/cm^2). An aqueous dispersion of the TiO_2/Cu:ZnS catalyst was deposited in the microreactor using a pipette and the microreactor was next heated to 70 °C until water was completely evaporated. 30 mg of the photocatalyst were deposited in the microreactor in each experiment.

Salicylic acid (SA) solution (10 mg/L) was injected by means of a syringe pump through the microreactor at a constant flow rate of 10 mL/h. SA can adsorb on TiO_2, which may result in a decrease in the solution concentration and the optical density of the solution. To take account of this background effect, we carried out the photodegradation reaction after flowing SA in the microreactor for 1.5 h in the dark to reach the adsorption equilibrium. The photocatalytic degradation of SA was initiated by irradiating the microreactor at 365 nm. The SA conversion was estimated by HPLC over the course of photocatalysis. After the chromatogram acquisition, the integration results give the output concentration of salicylic acid and then conversion yield. For each reaction time, final results were averaged out of at least three independent experiments. Less than 2.0% SA decomposed after 4 h in the absence of either the photocatalyst or the light irradiation and, thus, could be neglected in comparison with the SA degraded via photocatalysis.

3. Results and discussion

3.1. Synthesis and characterization of Cu:ZnS@MPA nanocrystals

An aqueous route was used to prepare Cu-doped ZnS QDs starting from $CuCl_2$, Na_2S and $ZnSO_4$ as precursors and using 3-mercaptopropionic acid (MPA) as surface ligand. An XPS analysis was first conducted to identify the oxidation state of copper in the Cu-doped ZnS nanocrystals. Fig. 1a shows the Cu $2p_{1/2}$ and Cu $2p_{3/2}$ signals which appear at 950.1 and 928.2 eV, respectively, and that can be assigned to a Cu(1+) oxidation state although Cu(2+) was used for the synthesis [36]. Cu^{2+} is a d^9 system with one unpaired electron and is paramagnetic, while Cu^+ being d^{10} system is diamagnetic [37]. The electron spin resonance (ESR) spectrum of the

Cu:ZnS@MPA QDs prepared with 3 mol% Cu relative to Zn exhibited no detectable ESR signal compared to that of a $CuCl_2$ aqueous solution with the same concentration, thus confirming that using our synthetic protocol, copper is incorporated in ZnS nanocrystals as Cu^+ [37,38]. This result is in agreement with previous reports where no ESR signal was observed for Cu-doped QDs and confirms that Cu^{2+} is reduced into Cu^+ probably by sulfide anions throughout the reaction evolution [37–39].

A representative transmission electron microscopy (TEM) image of Cu:ZnS@MPA QDs is shown in Fig. 1b. The average size of the nanocrystals is approximately 2.9 ± 0.5 nm, based on statistical analyses of more than 100 nanoparticles in a region (Fig. 1c). As can be seen, Cu:ZnS@MPA QDs are nearly monodispersed and of spherical shape. The wide angle XRD patterns of Cu:ZnS QDs exhibit the (1 1 1), (2 2 0), and (3 1 1) planes as shown in Fig. 1d, showing that nanocrystals are in the cubic zinc blende phase (JCPDS no 05-0566). The broadness of the peaks is due to the small size of the crystals. No diffraction peaks from impurities were detected in the sample. The diameter of Cu:ZnS particles, estimated using Rietveld refinements was found to be 3.0 ± 1.0 nm, which is in good agreement with the TEM measurements.

MPA-capped ZnS and Cu:ZnS QDs showed a broad absorption in the ultraviolet region. The first excitonic peak is located at 308 nm (4.02 eV) for both QDs (Fig. 2a). From the UV–vis data, the band gap values for a direct band gap semiconductor can be determined by the Tauc plot, $(\mathrm{Abs}.h\nu)^2$ versus $h\nu$, where Abs is the absorbance, h is Planck's constant, and ν is the frequency of the photon [40,41]. The Tauc plots are shown in Fig. 2b for ZnS and Cu:ZnS QDs. The bandgap determined (intersection of the sharply decreasing region with the baseline) is a decreasing function of the nanocrystalline size and was found to be 3.77 and 3.84 eV for ZnS and Cu:ZnS QDs, respectively, and confirms the quantum confinement regime of the dots.

Fig. 2c shows absorption and PL emission spectra of MPA-capped ZnS and Cu:ZnS QDs. For Cu:ZnS dots, a strong 500 nm PL band with a full-width at half-maximum of ca. 112 nm and a large Stokes shift of ca. 200 nm was observed. This blue-green emission is analogous to that observed in Cu-doped bulk samples [42–44] or to that previously described by others for Cu-doped ZnS or ZnSe QDs [45–48]. It originates from the displacement of photogenerated electrons to a shallow trap state associated with zinc dangling bonds or impurity donors such as halides or associated oxygen followed by its recombination with the hole-trapped d-state of Cu. This donor–acceptor recombination results in a PL emission located between 495 and 515 nm depending on the size of the host nanocrystals (blue shifting of the PL emission with decreasing the particle diameter). It is finally worth mentioning that undoped ZnS@MPA QDs prepared under the same conditions that the doped sample exhibit only a weak emission centered at 450–460 nm after excitation at 330 nm (Fig. 2c). This emission can be assigned to radiative recombination involving defects states in the ZnS nanocrystals based on the large Stokes shift from the bandgap energy.

As shown in Fig. 2d, the PL intensity of Cu:ZnS@MPA QDs increased during the first 5 min of irradiation with a Hg–Xe lamp

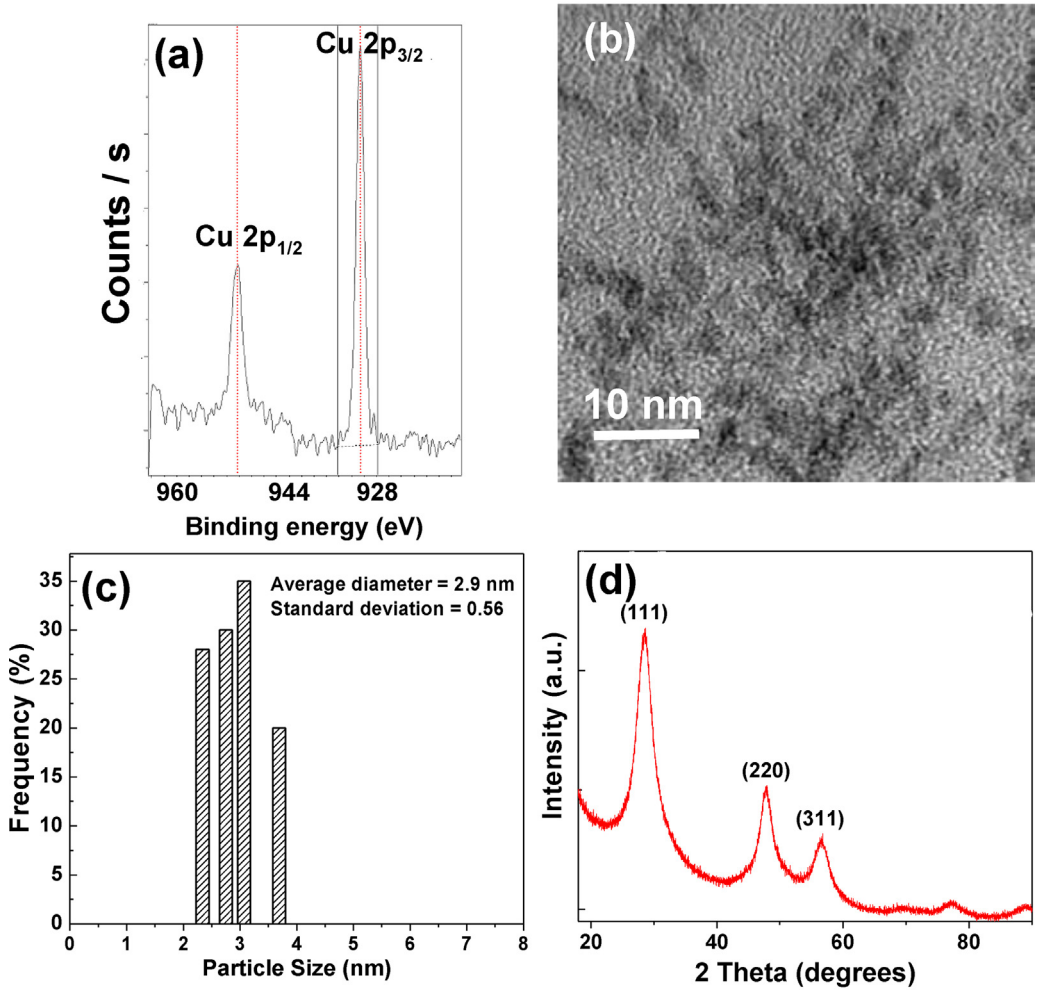

Fig. 1. (a) XPS spectrum of the Cu 2p peak, (b) TEM image of Cu:Zn@MPA quantum dots, (c) the corresponding size distribution, and (d) XRD pattern of the nanocrystals.

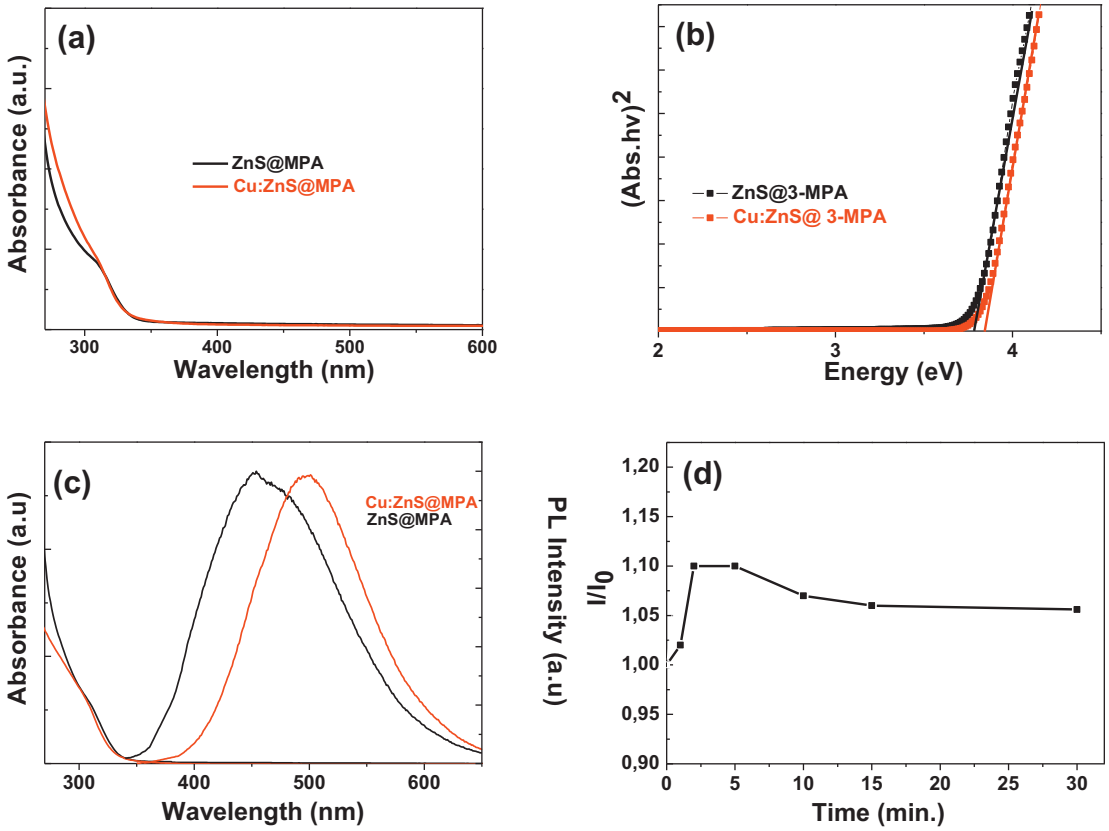

Fig. 2. (a) UV–visible absorption spectra of ZnS and Cu:ZnS nanocrystals, (b) Tauc plot for the absorption spectra depicted in Fig. 2a, (c) normalized absorption and PL emission spectra of Cu:ZnS@MPA QDs (red line) and ZnS@MPA QDs (black line), and (d) photostability of Cu:ZnS nanocrystals under irradiation of a Hg/Xe lamp (power = 200 mW). (For interpretation of the references to color in this artwork, the reader is referred to the web version of the article.)

(power = 200 mW) under ambient conditions and then leveled off at a constant value corresponding to ca. 105% of the initial value. That increase could be related to the photo-oxidation of the MPA surface ligand in the presence of light and oxygen, which leads to free sulfide ions that subsequently associate to Zn^{2+} to form a ZnS shell around the Cu:ZnS core. This limited ligand decomposition does neither induce aggregation nor shift in absorption and PL emission peaks, thus confirming the good colloidal stability and photostability of Cu:ZnS QDs.

TiO_2 is well-known to produce hydroxyl radicals (•OH) upon irradiation with UV light [49–51]. Using disodium terephthalate (DST) dosimetry, we also observed that Cu:ZnS@MPA QDs were able to produce •OH radicals. DST is known to react with •OH species in aqueous solution to generate 2-hydroxyterephthalate (OH-DST) that emits fluorescence at ca. 425 nm upon excitation at 312 nm [52,53]. Fig. 3a shows the evolution of OH-DST fluorescence spectra upon irradiation of 1 mL of Cu:ZnS QDs (ca. 8 mM) and 1 mL of DST (1 mM) with a Hg–Xe lamp (200 mW). After treatment of the irradiated samples with 1 M NaOH, the fluorescence intensity was measured. Control experiments 1 and 2, conducted without irradiation and with and without adding NaOH, respectively, demonstrate that •OH radical formation was photo-induced. Fig. 3b shows that the production of •OH radicals increased steadily during the 100 min irradiation of Cu:ZnS QDs. It is worth mentioning that the production of •OH radicals was lower using ZnS@MPA QDs and that it decreases with extended irradiation (after 60 min). These results show that Cu:ZnS QDs may not only serve to prevent fast e^-–h^+ recombination in TiO_2 but that these nanocrystals may also enhance •OH radicals production upon light activation (vide infra) and thus operate synergistically with TiO_2 for light-induced photooxidation.

3.2. Synthesis and characterization of TiO_2/Cu:ZnS nanocomposites

TiO_2/Cu:ZnS nanocomposites were next prepared by association of TiO_2 nanoparticles and Cu:ZnS@MPA QDs in aqueous solution at room temperature through self-assembly taking advantage of the carboxylate function of the MPA surface ligand. After centrifugation and washing with water, the powder obtained was further heated at 100 °C for 15 h to strongly associate the dots with TiO_2. XRD patterns showed that this heating does not modify the crystalline structure of TiO_2 (vide infra). As shown in Fig. 4a, the XRD pattern of P25 TiO_2 nanoparticles is composed of a mixed phase of the anatase and the rutile. The diffraction peaks at 2θ of 25.3°, 36.9°, 38.2°, 38.6°, 48.1°, 53.5°, 55.6°, 62.7°, and 75.0° are attributed to anatase-TiO_2 (JCPDF no 21-1272). The diffraction peaks of Cu:ZnS QDs were not detected on the XRD pattern due to the weak loading of QDs (1 wt% relative to TiO_2). Fig. 4b presents a TEM image of the nanocomposite. Cu:ZnS QDs could not be observed associated to TiO_2 by TEM but the related EDS analysis (Fig. 4c) indicates that TiO_2 and Cu:ZnS QDs co-exist in the nanocomposite and that the heterojunction between TiO_2 nanoparticles and the QDs has been constructed, which should improve the photocatalytic activity of the sample. Using EDS, the weight percent of Cu:ZnS QDs in the composite was found to 0.34%, value lower than the theoretical loading (1%). This may originate from the thermal decomposition of the MPA surface ligand during the drying phase and/or to the partial loss of Cu:ZnS QDs during the washing process.

The faint blue color of the TiO_2/Cu:ZnS composite compared to the white color of TiO_2 is in agreement with the bathochromic shift of the absorption spectrum to the visible range, as shown by the diffuse reflectance UV–vis spectra of the nanocomposite (Fig. 5a),

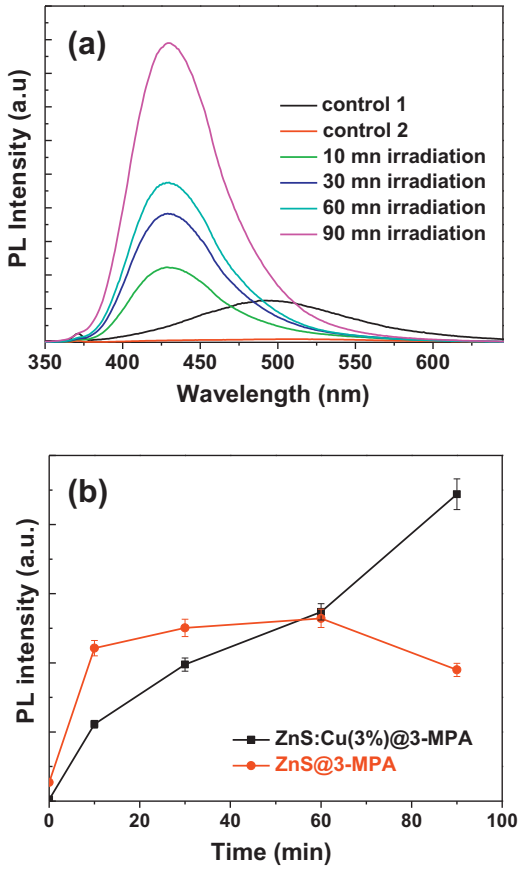

Fig. 3. (a) Typical PL emission spectra of 2-OH-DST obtained after photoactivation of Cu:ZnS QDs in the presence of DST, and (b) production of $OH^{\bullet}$ radicals by ZnS@MPA and Cu:ZnS@MPA QDs.

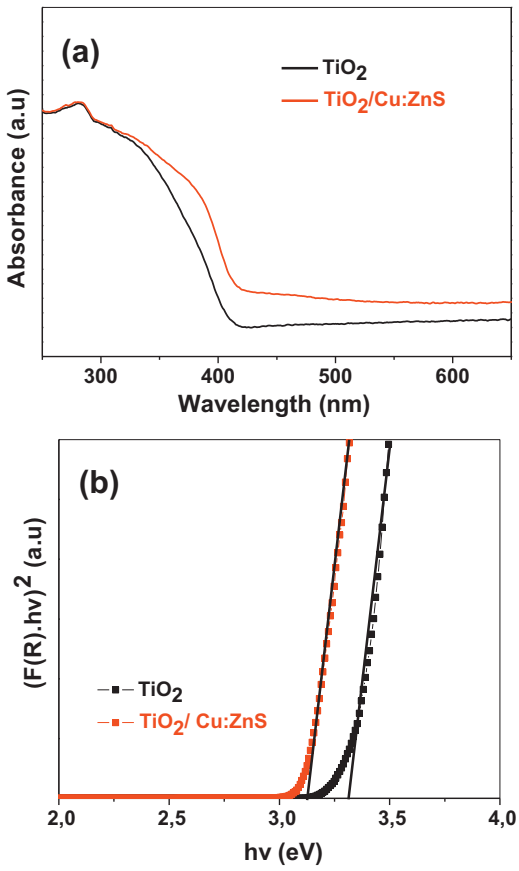

Fig. 5. (a) UV–vis diffuse reflectance spectra of TiO_2 nanoparticles and of the TiO_2/Cu:ZnS photocatalyst and (b) the corresponding Kubelka–Munk plots $(F(R).h\nu)^2$ versus photon energy ($h\nu$).

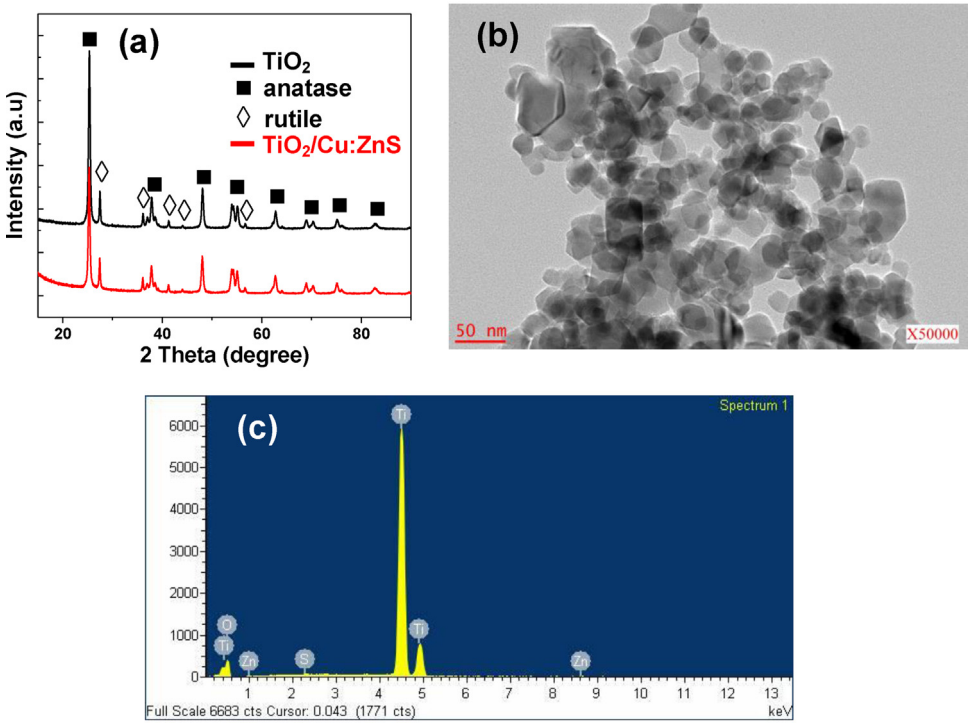

Fig. 4. (a) XRD patterns of TiO_2 (black) and of the TiO_2/Cu:ZnS nanocomposite (red), (b) TEM image and (c) EDX spectrum of the TiO_2/Cu:ZnS nanocomposite. (For interpretation of the references to color in this artwork, the reader is referred to the web version of the article.)

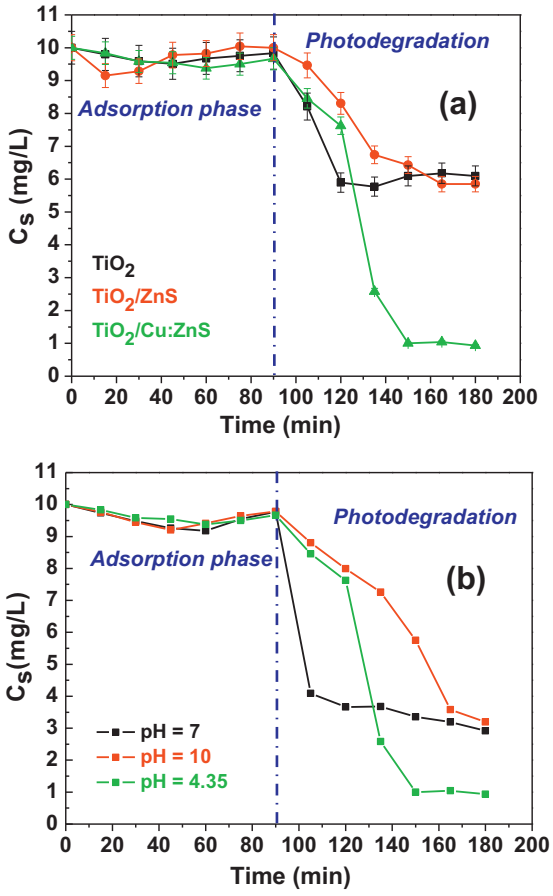

Fig. 6. Variations of salicyclic acid concentration (C_s) at the outlet of the microreactor during photocatalytic experiments using TiO_2, TiO_2/ZnS, and TiO_2/Cu:ZnS catalysts (a) at pH = 4.35 and (b) at pH values of 4.35, 7, and 10.

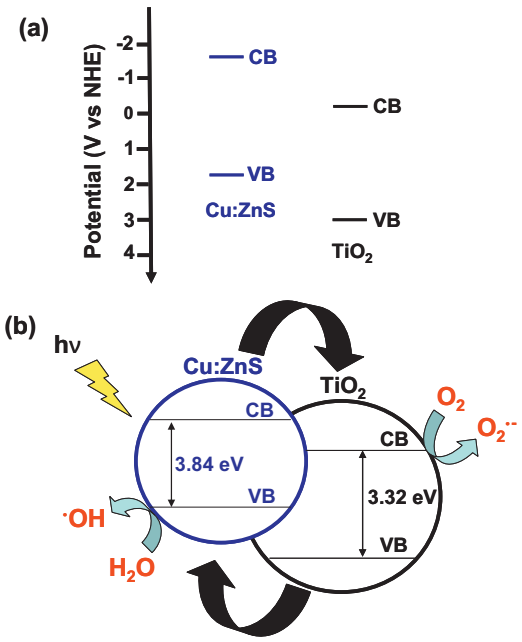

Fig. 7. (a) Schematic showing the thermodynamically favorable valence and conduction bands of Cu:ZnS QDs and of TiO_2, and (b) representation of the photogenerated electron–hole separation process in TiO_2/Cu:ZnS nanocomposites.

where the effect of Cu:ZnS QDs is clearly evidenced. The reflectance is maximum above ca. 420 nm and 440 nm for TiO_2 and TiO_2/Cu:ZnS materials, respectively. The Kubelka–Munk function was further used to evaluate the bandgap energy (E_g) of TiO_2 and TiO_2/Cu:ZnS particles (Fig. 5b) [54]. The shift of the gap to lower energy observed for the composite (E_g = 3.12 eV) compared to TiO_2 (E_g = 3.32 eV) probably originates from hybridization and strong electronic coupling of TiO_2 with Cu:ZnS QDs as previously observed for other photocatalysts like TiO_2/$CuInS_2$ [23] or TiO_2/CdS [13].

3.3. Evaluation of the photocatalytic activities of TiO_2/ZnS and TiO_2/Cu:ZnS nanocomposites

The photocatalytic activities of TiO_2, TiO_2/ZnS, and TiO_2/Cu:ZnS nanomaterials were determined using UV light irradiation and photodegradation experiments were conducted in microreactors. Salicylic acid (SA) was used as a test contaminant. After deposition of the photocatalysts, a solution of SA (10 mg L^{-1}) was continuously injected in the microreactor through a syringe pump. After an adsorption phase of 90 min, UV illumination was started and the concentration of SA at the outflow of the microreactor (C_s) was determined by HPLC. During the first 30 min of the experiments, it was observed that the photodegradation of SA over TiO_2 was faster than with TiO_2/ZnS or TiO_2/Cu:ZnS composites. About 40% SA was degraded over TiO_2, while only 20 and 15% SA were decomposed over TiO_2/ZnS and TiO_2/Cu:ZnS photocatalysts, respectively (Fig. 6a). However, after 60 min irradiation, ca. 90% of SA were photodegraded over TiO_2/Cu:ZnS, while bleaching of SA over TiO_2 or TiO_2/ZnS leveled off to a constant value of 40%. Nanocomposites were also prepared with increased loadings of Cu:ZnS QDs (2 or 3 wt% relative to TiO_2) but the degradation efficiencies were not enhanced significantly compared to experiments conducted with the nanocomposite prepared with 1 wt% of QDs.

TiO_2 is a n-type semiconductor [55,56], while Cu:ZnS a p-type semiconductor [57]. The bandgap of P25 TiO_2 used in this work is 3.32 eV [58], corresponding to an absorption threshold of 373 nm. So, when the nanocatalyst is activated under UV light irradiation (365 nm, 3.39 eV), both semiconductors are excited and e^-–h^+ pairs are generated in TiO_2 and in Cu:ZnS QDs. The electrons promoted in the conduction band of Cu:ZnS are transferred to the conduction band of TiO_2 and a high concentration of e^- is obtained in the CB band of TiO_2 compared to TiO_2 alone (Fig. 7a). These e^- react with O_2 to generate superoxide $O_2^{-\bullet}$ species. Simultaneously, the holes in the valence band of TiO_2 are transferred to the opposite direction to the valence band of Cu:ZnS QDs and generate hydroxyl radicals $^\bullet$OH upon reaction with adsorbed water molecules (Fig. 7b). This effective separation of e^-–h^+ pairs in TiO_2/Cu:ZnS nanocomposite originating from the p–n heterojunction between TiO_2 and Cu:ZnS is likely responsible of the increase of charge carriers lifetime and thus of the enhanced photocatalytic activity observed.

Effect of pH on the photocatalytic activity of the TiO_2/Cu:ZnS nanocomposite was finally investigated. Fig. 6b shows the photocatalytic efficiency of the nanocomposite at pH 4.35 (pH of the aqueous solution after solubilization of SA), at neutral pH, and at pH = 10, all of which are relevant for natural waters. NaOH was used to adjust the initial pH to 7 and 10. All photocatalytic tests were repeated three times. During the first 30 min of irradiation, the highest photocatalytic activity was observed at pH = 7. This activity weakens after 30 min and the degradation of SA is limited to ca. 70%. The highest degradation was observed at pH = 4.35 (90% conversion of SA after 60 min irradiation), while a basic pH decreases the performances of the TiO_2/Cu:ZnS photocatalyst. The pH-dependent kinetic and efficiencies of SA degradation observed are probably related to the TiO_2 surface charge and to the charge of SA versus pH and are in accordance with previous reports [59,60]. For P25 TiO_2, the point of zero charge (pzc) is close to 6.3. When photocatalytic experiments are run at pH higher than 6.3, adsorption

and thus degradation of SA are limited by the repulsion between the carboxylate function of SA and the negatively-charged surface of TiO_2. At pH lower than the pzc, the affinity of the carboxylate or carboxylic acid functions for the neutral TiO_2 surface probably improves adsorption, and hence degradation rates.

4. Conclusion

In summary, green-emitting MPA-capped Cu-doped ZnS quantum dots with an average diameter 2.9 ± 0.5 nm were successfully synthesized using a rapid and facile hydrothermal method. An interesting phenomenon is noted that the MPA-capped Cu:ZnS QDs have the ability to generate hydroxyl radicals upon UV light irradiation. Integration of p-type Cu:ZnS QDs with n-type TiO_2 to form a p–n heterojunction was next achieved by a thermal treatment process. The photocatalytic activities of TiO_2 nanoparticles and of TiO_2/ZnS and TiO_2/Cu:ZnS nanocomposites have been investigated under UV light illumination. The TiO_2/Cu:ZnS material was found to have the highest photocatalytic performance for the degradation of salicylic acid. The enhanced photocatalytic activity of the TiO_2/Cu:ZnS nanocomposite compared to TiO_2/ZnS and to TiO_2 probably originates from the synergetic effects of (i) an effective electron–hole pairs separation by the p–n heterojunction constructed by n-type TiO_2 and p-type Cu:ZnS and (ii) the ability of Cu:ZnS dots to generate hydroxyl radicals and to behave as a co-catalyst once associated to TiO_2 and thus increase its oxidizing capacity.

Acknowledgement

We thank Pr. Jacques Lalevée, Institut de Science des Matériaux de Mulhouse (IS2M), Mulhouse, France, for ESR experiments.

References

[1] D. Beydoun, R. Amal, G. Low, S. Mcevoy, Journal of Nanoparticles Research 1 (1999) 439–458.
[2] W.F. Zhou, Q.J. Liu, Z.Q. Zhu, J. Zhang, Journal of Physics D: Applied Physics 43 (2010), 035301 (6 pp.).
[3] E. Sthathatos, D. Tsiourvas, P. Lianos, Journal of Colloids and Surfaces A: Physicochemical Engineering Aspects 149 (1999) 49–56.
[4] R. Comparelli, E. Fanizza, M.L. Curri, P.D. Cozzoli, G. Mascolo, R. Passino, A. Agostiano, Applied Catalysis B: Environmental 55 (2005) 81–91.
[5] S. Kaniyankandy, H.N. Ghosh, Journal of Materials Chemistry 19 (2009) 3523–3528.
[6] M. Anpo, T. Shima, S. Kodawa, Y. Kubokawa, Journal of Physical Chemistry 91 (1987) 4305–4310.
[7] K. Tanaka, M.F.V. Capule, T. Hisanage, Chemical Physics Letters 187 (1991) 73–76.
[8] A. Sclafani, J.M. Herrmann, Journal of Physical Chemistry 100 (1996) 13655–13661.
[9] Y.S. Chen, J.C. Crittenden, S. Hackney, L. Sutter, D.W. Hand, Environmental Science and Technology 39 (2005) 1201–1208.
[10] Y.J. Kim, B. Gao, S.Y. Han, M.H. Jung, A.K. Chakraborty, T. Ko, C. Lee, W.I. Lee, Journal of Physical Chemistry C 113 (2009) 19179–19184.
[11] P.A. Sant, P.V. Kamat, Physical Chemistry Chemical Physics 4 (2002) 198–203.
[12] W.-T. Sun, Y. Yu, H.-Y. Pan, X.-F. Gao, Q. Chen, L.-M. Peng, Journal of the American Chemical Society 130 (2008) 1124–1125.
[13] S. Banerjee, S.K. Mohapatra, P.P. Das, M. Misra, Chemistry of Materials 20 (2008) 6784–6791.
[14] G.-S. Li, D.-Q. Zhang, J.C. Yu, Environmental Science and Technology 43 (2009) 7079–7085.
[15] Z.-X. Lu, Z.-L. Zhang, M.-X. Zhang, H.-Y. Xie, Z.-Q. Tian, P. Chen, H. Huang, D.-W. Pang, Journal of Physical Chemistry B 109 (2005) 22663–22666.
[16] R.S. Dibbell, G.R. Soja, R.M. Hoth, D.F. Watson, Langmuir 23 (2007) 3432–3439.
[17] C. Harris, P.V. Kamat, ACS Nano 3 (2009) 682–690.
[18] C. Ratanatawanate, C. Xiong, K.J. Balkus Jr., ACS Nano 2 (2008) 1682–1688.
[19] B. Ma, L. Wang, H. Dong, R. Gao, Y. Geng, Y. Zhu, Y. Qiu, Physical Chemistry Chemical Physics 13 (2011) 2656–2658.
[20] C. Wang, R.L. Thompson, P. Ohodnicki, J. Baltrus, C. Matranga, Journal of Materials Chemistry 21 (2011) 13452–13457.
[21] K.P. Acharya, T.R. Alabi, N. Schmall, N.N. Hewa-Kasakarage, M. Kirsanova, A. Nemchinov, E. Khon, M. Zamkov, Journal of Physical Chemistry C 113 (2009) 19531–19535.
[22] C. Wang, K.-W. Kwon, M.L. Odlyzka, B.H. Lee, M. Shim, Journal of Physical Chemistry C 111 (2007) 11734–11741.
[23] F. Shen, W. Que, Y. Liao, X. Yin, Industrial & Engineering Chemistry Research 50 (2011) 9131–9137.
[24] J.S. Jang, P.H. Borse, J.S. Lee, S.H. Choi, H.G. Kim, Journal of Chemical Physics 128 (2008), 154717 (6 pp.).
[25] M. Kanemoto, H. Hosokawa, Y. Wada, K. Murakoski, S. Yanagida, T. Sakara, H. Mori, M. Ishikawa, H. Kobayashi, Journal of the Chemical Society, Faraday Transactions 92 (1996) 2401–2411.
[26] A.L. Stroyuk, A.E. Raevskaya, A.V. Korzhak, S.Y. Kuchmii, Journal of Nanoparticles Research 9 (2007) 1027–1039.
[27] J.-S. Hu, L.-L. Ren, Y.-G. Guo, H.-P. Liang, A.-M. Cao, L.-J. Wan, C.-L. Bai, Angewandte Chemie International Edition 44 (2005) 1269–1273.
[28] V. Stengl, S. Bakardjieva, N. Murafa, V. Houskova, K. Lang, Microporous and Mesoporous Materials 110 (2008) 370–378.
[29] A. Franco, M.C. Neves, M.M.L. Ribeiro Carrott, M.H. Mendonça, M.I. Pereira, O.C. Monteiro, Journal of Hazardous Materials 161 (2009) 545–550.
[30] Y. Xiaodan, W. Qingyin, J. Shicheng, G. Yihang, Materials Characterization 57 (2006) 333–341.
[31] A. Kudo, M. Sekizawa, Catalysis Letters 58 (1999) 241–243.
[32] H.R. Pouretedal, H. Beigy, M.H. Keshavarz, Environmental Technology 31 (2010) 1183–1190.
[33] A. Aboulaich, L. Balan, J. Ghanbaja, G. Medjahdi, C. Merlin, R. Schneider, Chemistry of Materials 23 (2011) 3706–3713.
[34] M. Geszke-Moritz, H. Piotrowska, M. Murias, L. Balan, M. Moritz, J. Lulek, R. Schneider, Journal of Materials Chemistry B 1 (2013) 698–706.
[35] G. Charles, T. Roques-Carmes, N. Becheikh, L. Falk, J.M. Commenge, S. Corbel, Journal of Photochemistry and Photobiology A: Chemistry 223 (2011) 202–211.
[36] R. Lopez, R. Gomez, M.E. Llanos, Catalysis Today 148 (2009) 103–108.
[37] C. Corrado, Y. Jiang, F. Oba, M. Kozina, F. Bridges, J. Zhang, Journal of Physical Chemistry A 113 (2009) 3830–3839.
[38] B.B. Srivastasa, S. Jana, N. Pradhan, Journal of the American Chemical Society 133 (2011) 1007–1015.
[39] B. Car, S. Medling, C. Corrado, F. Bridges, Z.J. Zhang, Nanoscale 3 (2011) 4182–4189.
[40] J. Tauc, A. Menth, Journal of Non-Crystalline Solids 569 (1972) 8–10.
[41] M. Moffitt, A. Eisenberg, Chemistry of Materials 7 (1995) 1178–1184.
[42] M. Godlewski, W. Lamb, B. Cavenett, Solid State Communications 39 (1981) 595–599.
[43] G. Jones, J. Woods, Journal of Luminescence 9 (1974) 389–405.
[44] M. Godlewski, W. Lamb, B. Cavenett, Journal of Luminescence 24 (1981) 173–176.
[45] N. Pradhan, D. Goorskey, J. Thessing, X. Peng, Journal of the American Chemical Society 127 (2005) 17586–17587.
[46] C. Corrado, Y. Jiang, F. Oba, M. Kozina, F. Bridges, J.Z. Zhang, Journal of Physical Chemistry A 113 (2009) 3830–3839.
[47] S. Jana, B.B. Srivestava, S. Acharya, P.K. Santra, N.R. Jana, D. Sarma, N. Pradhan, Chemical Communications 46 (2010) 2853–2855.
[48] S. Gul, J.K. Cooper, C. Corrado, B. Vollbrecht, F. Bridges, J. Guo, J.Z. Zhang, Journal of Physical Chemistry C 115 (2011) 20864–20875.
[49] C.S. Turchi, D.F. Ollis, Journal of Catalysis 122 (1990) 178–192.
[50] A.L. Linsebigler, G. Lu, J.T. Yates, Chemical Reviews 95 (1995) 735–758.
[51] R. Gao, J. Stork, D.W. Bahnemann, J. Rabani, Journal of Photochemistry and Photobiology A: Chemistry 148 (2002) 387–391.
[52] J.T. Mason, P.J. Lorimer, M.D. Bates, Y. Zhao, Ultrasonics Sonochemistry 1 (1994) S91–S95, 1194.
[53] B.I. Ipe, M. Lehning, C.M. Niemeyer, Small 1 (2005) 706–709.
[54] M.K. Arora, N. Sahu, S.N. Upadhyay, A.S.K. Sinha, Industrial & Engineering Chemistry Research 38 (1999) 2659–2665.
[55] L. Forro, O. Chauvet, D. Emin, L. Zuppiroli, H. Berger, F. Lévy, Journal of Applied Physics 75 (1994) 633–635.
[56] C. Di Valentin, G. Pacchioni, A. Selloni, Journal of Physical Chemistry C 113 (2009) 20543–20552.
[57] M. Shim, P. Guyot-Sionnest, Nature 407 (2000) 981–983.
[58] A. Hagfeldt, M. Grätzel, Chemical Reviews 95 (1995) 49–68.
[59] A. Piscopo, D. Robert, J.V. Weber, Applied Catalysis B: Environmental 35 (2001) 117–124.
[60] A. Di Paola, G. Marci, L. Palmisano, M. Schiavello, K. Uosaki, S. Ikeda, B. Ohtani, Journal of Physical Chemistry B 106 (2002) 637–645.